

Long-distance entanglement in many-body atomic and optical systems

Salvatore M. Giampaolo^{1,2} and Fabrizio Illuminati^{1,2,3}

¹*Dipartimento di Matematica e Informatica, Università degli Studi di Salerno,
Via Ponte don Melillo, I-84084 Fisciano (SA), Italy*

²*CNR-INFM Coherentia, Napoli, Italy; CNISM Unità di Salerno; and INFN Sezione di Napoli,
Gruppo collegato di Salerno, Baronissi (SA), Italy*

³*ISI Foundation for Scientific Interchange, Villa Gualino, Viale Settimio Severo 65, I-10133 Torino, Italy*

(Dated: November 19, 2009)

We discuss the phenomenon of long-distance entanglement in the ground state of quantum spin models, its use in high-fidelity and robust quantum communication, and its realization in many-body systems of ultracold atoms in optical lattices and in arrays of coupled optical cavities. We investigate XX quantum spin models on one-dimensional lattices with open ends and different patterns of site-dependent interaction couplings, singling out two general settings: Patterns that allow for perfect long-distance entanglement (LDE) in the ground state of the system, namely such that the end-to-end entanglement remains finite in the thermodynamic limit, and patterns of quasi long-distance entanglement (QLDE) in the ground state of the system, namely, such such that the end-to-end entanglement vanishes with a very slow power-law decay as the length of the spin chain is increased. We discuss physical realizations of these models in ensembles of ultracold bosonic atoms loaded in optical lattices. We show how, using either suitably engineered super-lattice structures or exploiting the presence of edge impurities in lattices with single periodicity, it is possible to realize models endowed with nonvanishing LDE or QLDE. We then study how to realize models that optimize the robustness of QLDE at finite temperature and in the presence of imperfections using suitably engineered arrays of coupled optical cavities. For both cases the numerical estimates of the end-to-end entanglement in the actual physical systems are thoroughly compared with the analytical results obtained for the spin model systems. We finally introduce LDE-based schemes of long-distance quantum teleportation in linear arrays of coupled cavities and show that they allow for high-fidelity and high success rates even at moderately high temperatures.

PACS numbers: 03.67.Hk, 03.67.Mn, 75.10.Pq

I. INTRODUCTION

Quantum entanglement plays a crucial role in many areas of quantum information science [1], including, among others, quantum cryptography and secure quantum key distribution [2], and quantum communication [3]. For this reason, much work has been dedicated to single out ways to produce useful entanglement for efficient and robust implementation of quantum information tasks. The most natural way to create entanglement between two or more constituents of a quantum information device appears to be by means of direct interactions because, intuitively, large amounts of entanglement should be associated to the presence of strong quantum correlations. However, from a general quantum informatic perspective, an even more desirable goal is to envisage ways to produce large amounts of entanglement shared between distant and generally not directly interacting constituents. Along the way to accomplish this task, a first step has been realized by introducing the concept of localizable entanglement [4], namely the rate of entanglement that can be concentrated on a pair of arbitrarily distant constituents by performing optimal local measurements onto the remainder of the system. More recently, it has been shown that the ground state of some spin models with finite correlation length defined on one-dimensional chains with open ends can support large values of the end-to-end entanglement between the initial and final points of the

chain, insensitive or only very weakly sensitive to the size of the system[5, 6, 7, 8]. This type of entanglement has thus been dubbed Long-Distance Entanglement (LDE). In this approach, the guiding principle is to look for systems whose GS can support *intrinsically* large amounts of (long-distance) entanglement, even at moderately high temperatures and in the presence of bulk imperfections, without the need for performing operations and measurements or for continuous dynamical controls and adjustments of the couplings. Clearly, the property of LDE would be very appealing in the quest to design quantum information devices, that perform tasks efficiently and at the same time are sufficiently robust against decoherence, based on (properly engineered) many-body systems of condensed matter that could possibly be realized with currently available technologies, or technologies that may be in view in the near future.

The scope of the present work is to investigate various theoretical aspects of the phenomenon of LDE in quantum many-body physics, to introduce possible concrete experimental implementations with currently available many-body systems of atomic physics and quantum optics, and to discuss simple schemes of LDE-based efficient and robust quantum communication. Concerning the theoretical modeling, here and in the following we will consider as paradigmatic test-beds some very simple isotropic quantum spin models on open chains with XX -type interactions of site-dependent strength. For suit-

able choices of the sets of site-dependent couplings, these models can show large values of the entanglement shared by the end spins of the chain [7, 8]. Notwithstanding their apparent simplicity, they are a very powerful and useful tool in order to investigate, identify, classify, and summarize the different possible types of LDE, and the properties associated to different patterns of site-dependent interaction strengths. Moreover, these different classes of XX quantum spin models with site-dependent interaction couplings turn out to be very well suited to assess the experimentally relevant problem of the vanishing of the energy gap as a function of the size of the system, and to identify, unambiguously, the optimal range of parameters compatible with the largest achievable value of LDE at fixed values of the temperature and of the length of the chain.

After establishing the general theoretical framework, we will analyze some possible realizations based on two many-body systems of current experimental interest and that are moreover evolving and being developed at a fast pace, namely systems of ultracold neutral atoms in optical lattices [9] and arrays of coupled cavities [10]. These two systems share some common features. They can be seen as ensembles of local structures that interact with each other via the exchange of bosonic particles, atoms in the case of optical lattices, and photons in the case of coupled cavities. Both systems allow to simulate quantum spin models by effectively reducing the dimension of the local state space, and by realizing spin-spin interactions via the inter-site hopping amplitudes. However, while the hopping amplitude in an array of coupled optical microcavities can be tuned at will, at least in principle, either by adjusting the inter-cavity overlaps and/or by tuning the cavities' fundamental physical parameters (Rabi couplings, quality factors, etc.) of every single cavity (single-site addressing), this task appears to be much more challenging in optical lattices, for which the inter-site properties are indissolubly woven with the frequency of the external laser potentials, and hence site-dependent interactions between the effective spins can be engineered either by introducing atomic impurities and/or by designing super-lattice structures. We will discuss merits and disadvantages of both types of systems in the quest for the experimental demonstration of LDE and its use in the realization of efficient, robust, and high-fidelity quantum information tasks.

The paper is organized as follows: In Section II we introduce the general XX spin chain Hamiltonian with arbitrary site-dependent couplings and review the methods to determine its spectrum, its ground-state properties, and the end-to-end concurrence. In Section III we investigate the properties of LDE for different patterns of site-dependent interaction couplings, singling out two different general situations: Patterns that allow for perfect LDE, namely such that the end-to-end entanglement remains finite in the limit of diverging size of the system, and quasi-LDE (or imperfect LDE), i.e. such that the end-to-end entanglement vanishes with a very slow

power-law decay as the length of the chain increases. In Section IV we discuss how to realize or, better, how to simulate the models analyzed in Section III with ensembles of ultracold bosonic atoms loaded in optical lattices. In the literature there exist several proposals to implement LDE-free spin models, either with uniform [11, 12, 13] or random [14] spin-spin couplings, using optical lattices in various settings. Here we show how, using either suitably engineered super-lattice structures or exploiting the presence of edge impurities in lattices with single periodicity, it is possible to realize models endowed with nonvanishing LDE in the ground state. In section V we investigate how to realize spin models supporting LDE by the use of suitable array structures of coupled cavities. In fact, these systems are being intensively studied in relation to their ability to realize/simulate collective phenomena typical of strongly correlated systems of condensed matter [10, 15, 16, 17, 18, 19]. Concerning the simulation of spin models, we show how, at least in principle, this type of system allows to simulate straightforwardly XX models with arbitrary patterns of site-dependent couplings and different types of LDE. In both sections numerical estimates of the end-to-end entanglement in the actual physical systems are thoroughly compared with the results obtained in the simulated spin model systems. In Section VI we discuss the implementation of an LDE-based scheme of long-distance quantum teleportation exploiting open linear arrays of coupled cavities. In particular, we show that this scheme allows for high-fidelity teleportation even at moderately high temperatures and in the presence of noise. Finally, in the conclusions we summarize our findings and discuss some outlooks on possible future developments along this line of research.

II. GENERAL STRUCTURE OF XX QUANTUM SPIN MODELS ON OPEN CHAINS

As anticipated in the introduction, in this Section we discuss the properties of XX quantum spin-1/2 models defined on one-dimensional lattices with open ends, with specific patterns of nearest-neighbor interactions. Such models are all special instances of the general XX Hamiltonian

$$H_{XX} = \sum_{i=1}^{N-1} J_i (S_i^x S_{i+1}^x + S_i^y S_{i+1}^y) , \quad (1)$$

where J_i is the interaction strength between spins at nearest neighboring sites i and $i+1$, S_i^α is the spin-1/2 operator defined at site i , and N is the total number of sites (spins) or, equivalently, the length of the chain. The spectrum of this Hamiltonian can be determined exactly by a straightforward generalization of the methods first discussed by Lieb, Schultz, and Mattis [20]. The first step in the procedure is to perform a Jordan-Wigner transfor-

mation [21],

$$\begin{aligned} S_i^+ &= c_i^\dagger e^{i\pi \sum_{j=1}^{i-1} c_j^\dagger c_j}, & S_i^- &= e^{-i\pi \sum_{j=1}^{i-1} c_j^\dagger c_j} c_i, \\ S_i^z &= c_i^\dagger c_i - \frac{\mathbb{I}}{2}, \end{aligned} \quad (2)$$

where $S_j^\pm = S_j^x \pm iS_j^y$. As a result, the Hamiltonian (1) is mapped in the free fermion Hamiltonian

$$H = \frac{1}{2} \sum_{i=1}^{N-1} J_i (c_i^\dagger c_{i+1} + c_{i+1}^\dagger c_i) = \mathbf{c}^\dagger M \mathbf{c}, \quad (3)$$

where $\mathbf{c}^\dagger = (c_1^\dagger, \dots, c_N^\dagger)$ (\mathbf{c}) is the vector of the N fermionic creation (annihilation) operators, one for each site of the lattice, and the adjacency matrix M reads

$$M = \frac{1}{2} \begin{vmatrix} 0 & J_1 & 0 & \cdots & 0 \\ J_1 & 0 & J_2 & & \\ 0 & J_2 & 0 & & \vdots \\ \vdots & & \ddots & J_{N-2} & 0 \\ 0 & \cdots & 0 & J_{N-1} & 0 \end{vmatrix}. \quad (4)$$

Given the GS of the system, we are interested in the evaluation of the end-to-end entanglement in the reduced two-qubit state between the first spin at site 1 and the last spin at site N . One thus needs to determine the spin-spin concurrence (entanglement of formation) between the end points of the chain. This quantity can be computed exactly for any two-qubit state (pure or mixed), thanks to the celebrated Wootters formula [22], and the task is left to obtain its explicit expression in the reduced state of the two end-point spins. To this purpose, we need to calculate explicitly all the possible forms of two-point correlations in the GS. The Hamiltonian (1) is symmetric under rotations of the spins around the z -axis, so that the only nonvanishing correlations are $\langle S_i^x S_j^x \rangle = \langle S_i^y S_j^y \rangle$, $\langle S_i^z S_j^z \rangle$ and $\langle S_i^z \rangle$. In the absence of external magnetic fields, π -rotations around the x and y axes are symmetries of the model, which additionally implies $\langle S_i^z \rangle = 0$ at every site. Thanks to the aforementioned symmetries, the two-point reduced density matrix $\rho_{i,j}$, obtained by tracing the ground-state density matrix of the entire system over all spins except the ones at sites $\{i, j\}$, has the form

$$\rho_{i,j} = \frac{\mathbb{I}}{4} + \langle S_i^x S_j^x \rangle (\sigma^x \otimes \sigma^x + \sigma^y \otimes \sigma^y) + \langle S_i^z S_j^z \rangle \sigma^z \otimes \sigma^z, \quad (5)$$

where $\sigma^{x,y,z}$ are the Pauli matrices and $\langle \cdot \rangle$ is the GS average at temperature $T = 0$, or the thermal one at finite temperature $\beta = (k_B T)^{-1}$ with respect to the Gibbs state $\rho = e^{-\beta H} Z^{-1}$. We are interested in the case in which $i = 1$ and $j = N$ are the two end points of the chain. In this instance, we have

$$\begin{aligned} S_1^+ S_N^- + S_1^- S_N^+ &= -e^{i\pi \mathcal{N}} (c_1^\dagger c_N + c_N^\dagger c_1), \\ S_1^z S_N^z &= \left(c_1^\dagger c_1 - \frac{1}{2} \right) \left(c_N^\dagger c_N - \frac{1}{2} \right), \end{aligned} \quad (6)$$

where $\mathcal{N} = \sum_{i=1}^N c_i^\dagger c_i$ is the total number operator. Applying Wick's theorem and taking into account that $\langle c_i^\dagger c_i \rangle = 1/2$, we obtain

$$\begin{aligned} \langle S_1^+ S_N^- + S_1^- S_N^+ \rangle &= -e^{i\pi \mathcal{N}/2} (\langle c_1^\dagger c_N \rangle + \langle c_N^\dagger c_1 \rangle), \\ \langle S_1^z S_N^z \rangle &= -\langle c_1^\dagger c_N \rangle \langle c_N^\dagger c_1 \rangle. \end{aligned} \quad (7)$$

Setting $x \equiv \langle c_1^\dagger c_N \rangle$ we see that the end-to-end reduced density matrix depends uniquely on this parameter. For reduced states of the form (5) the end to end concurrence $C_{1,N}$ is readily computed [23]. In our case, we have

$$C_{1,N} = 2 \max \left\{ 0, x^2 + |x| - \frac{1}{4} \right\}. \quad (8)$$

The concurrence is thus nonvanishing for $|x| > (\sqrt{2} - 1)/2 \simeq 0.207$, and it reaches the maximum value $C_{1,N} = 1$ for $|x| \rightarrow 1/2$.

It is natural to expect that the existence of a strong quantum correlation between the two end spins of the chain can be conveniently exploited for performing tasks in quantum information, in particular considering teleportation schemes. In the standard quantum teleportation protocol, two parties A and B share a maximally entangled state (Bell state). Party A holds also a third qubit, whose unknown state is to be teleported. If the two end points of our XX chain share a highly entangled state, that in some limit may even be asymptotically close to a Bell state, they can be identified as the two parties, sender and receiver, for a long-distance, high-fidelity teleportation protocol. The efficiency of a quantum channel in teleporting an unknown state is quantified by the fidelity f between the output and the input states, averaged over all input realizations. The fidelity depends on the actual properties of the entangled resource $\rho_{1,L}$ (Cfr. Eq. (5)) shared by the end spins of the chain. In fact, it has been demonstrated that the optimal fidelity depends only on the “fully entangled fraction” F_{full} , according to the formula $f = (2F_{full} + 1)/3$ [24]. The fully entangled fraction is defined as the fidelity between the resource $\rho_{1,L}$ and a maximally entangled state, maximized over all possible maximally entangled states. For states of the form Eq. (5) it can be easily computed, and reads $F_{full} = \frac{1}{4} + |x| + x^2$ [25]. The associated teleportation fidelity is thus

$$f = \frac{2(\frac{1}{4} + |x| + x^2) + 1}{3}, \quad (9)$$

and, taking into account Eq. (8), from Eq. (9) we obtain the expression of the concurrence $C_{1,N}$ as a function of the fidelity:

$$C_{1,N} = 2 \max \left\{ 0, \frac{3}{2} f - 1 \right\}. \quad (10)$$

This expression highlights the crucial interplay between entanglement and efficiency in quantum information protocols. In fact, due to the high symmetry of states of

the form Eq. (5), a nonvanishing entanglement implies a nonclassical teleportation fidelity exceeding the classical threshold 2/3, and viceversa. Moreover the relation between the maximum fidelity that can be obtained in a quantum teleportation between the end points of the spin chain and the end-to-end Eq. (10) provides a simple route to probe, via experimental implementations of quantum teleportation protocols, the actual values of the generated long-distance entanglement $C_{1,N}$.

All the physical information about model (3) can now be obtained by diagonalizing the one-body matrix M . Let ξ_k be the eigenvector of M with eigenvalue Λ_k , where k is a quasi-momentum label. Passing to new fermionic operators via the transformation $c_i = \sum_k \xi_k^{(i)} c_k$, the Hamiltonian takes the form

$$H_{XX} = \sum_k \Lambda_k c_k^\dagger c_k. \quad (11)$$

The evaluation of the two-point correlation x is finally straightforward:

$$\begin{aligned} x &= \sum_{k,q} \xi_k^{(1)} \xi_q^{(N)} \langle c_k^\dagger c_q \rangle \\ &= \begin{cases} \sum_{\Lambda_k < 0} \xi_k^{(1)} \xi_k^{(N)} & \text{for } T = 0 \\ \sum_k \xi_k^{(1)} \xi_k^{(N)} \frac{1}{1 + e^{\beta \Lambda_k}} & \text{for } T > 0, \end{cases} \end{aligned} \quad (12)$$

where x depends on the set of the couplings J_i as well as on the temperature T , whenever $T \neq 0$.

In conclusion, the full evaluation of the end-to-end entanglement in XX quantum spin models defined on open chains, with arbitrary patterns of site-dependent nearest-neighbor interactions, is strictly associated to the complete diagonalization of the M matrix in Eq.(4). While in some particular cases it is possible to find the exact analytic expressions of the eigenvalues and of the eigenvectors of M [7, 26], in the most general case the problem has to be solved by exact numerical diagonalization.

III. END-TO-END ENTANGLEMENT PROPERTIES OF XX SPIN CHAINS

Having reviewed the basic definitions and mathematical tools needed to analyze the end-to-end entanglement properties in XX spin chains with arbitrary site-dependent interaction strengths, we need to look for those sets of couplings that allow for large values of LDE, possibly robust against thermal decoherence and bulk imperfections. The required entanglement properties. The basic idea for concentrating a large amount of entanglement on the two end spins of the chain is inspired by the observation that for some frustration-free systems, like the antiferromagnetic Heisenberg model [5, 6], and some XX -type models [7, 8], the total energy is minimized by states tending to form a global singlet. This fact, together with the property of monogamy for bipartite entanglement [27], is the primary cause for the

phenomenon of LDE. Namely, if one selects a set of interaction couplings in the Hamiltonian Eq.(1) that are such to forbid the end spins to entangle with any other constituents, then, by monogamy, strong quantum correlations will develop between them.

A. Perfect Long Distance Entanglement (LDE)

In analogy with the case of the dimerized antiferromagnetic Heisenberg chain, that was the system in which the phenomenon of LDE was first discovered [5], we begin by reviewing the properties of the XX spin chain with bonds of alternating strengths, i.e. a model in which each weak bond ($J_{k-1} = \lambda J$, with $\lambda \ll 1$) between neighboring spins at sites is followed by a much stronger one ($J_k = J$) between the successive pair of neighboring spins. This model has been introduced and investigated in Ref. [7]. If the chain is formed of an even number of sites and the two end points are coupled to their nearest neighbors with a weak bond, this model fulfills exactly the requirements needed in order to establish perfect LDE between the end spins of the chain. Namely, any spin in the chain but the end ones is subject to a weak (left) interaction and to a strong (right) interaction. Hence, every spin in the bulk tends to be maximally entangled with its strongly interacting neighbor. Each of the two end spins is subject only to a weak bond interaction, and is therefore excluded from the arrangement in pairs of nearest-neighbor singlets due to the monogamy property of bipartite entanglement [27]. Furthermore, because the GS of the model tends to be a collection of singlets, the two end spin spins are effectively coupled and develop a nonvanishing LDE mediated by the remainder of the chain, notwithstanding the fact that they do not interact directly in any way.

The above qualitative reasoning can be made precise and quantitative. The Hamiltonian for the XX spin model with alternating weak and strong interactions is

$$H = \frac{J}{2} \sum_{i=1}^{N-1} [(1 + \lambda) + (-1)^i (1 - \lambda)] (S_i^x S_{i+1}^x + S_i^y S_{i+1}^y). \quad (13)$$

Following the approach described in the previous section, one can determine the end-to-end concurrence for different values of λ and different lengths of the chain [7], as shown in Fig. 1. We can see that as the weak coupling λ decrease below a threshold value $\lambda_c = 0.765$ [7], a nonvanishing concurrence begins to develop. For a fixed length of the chain, decreasing λ still further (and thus increasing the difference between the alternating couplings) allows the creation of dimers between pairs of strongly interacting neighboring spins. The dimers, in turn, are very weakly coupled to each other. Hence, because the two end spins of the chain interact very weakly with their nearest neighbors, dimerization and monogamy of entanglement force the creation of a strong quantum correlation between the end points, in analogy with what hap-

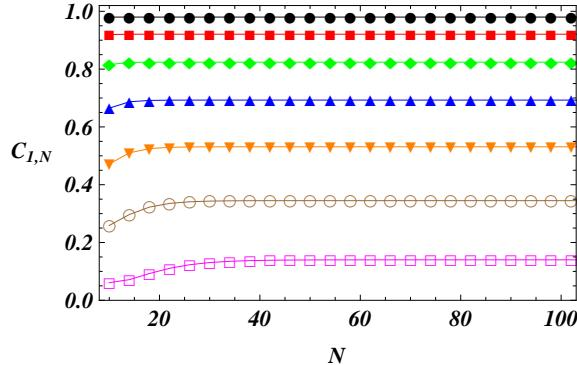


Figure 1: End-to-end concurrence $C_{1,N}$ for the 1-D XX spin model with alternating couplings described by the Hamiltonian Eq.13, plotted as a function of the number of lattice sites N (length of the chain), for different value of the weak coupling λ . From bottom to top: magenta empty squares: $\lambda = 0.7$; brown empty circles: $\lambda = 0.6$; orange inverted triangles: $\lambda = 0.5$; blue triangles: $\lambda = 0.4$; green diamonds: $\lambda = 0.3$; red full squares: $\lambda = 0.2$; black full circles: $\lambda = 0.1$.

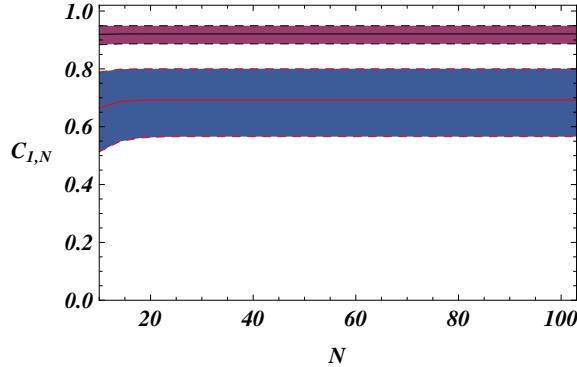


Figure 2: End-to-end entanglement as a function of the length of the chain for the model with noisy couplings described by Eq. (15), where χ_i is a random variable uniformly distributed in the interval $\{-\bar{\chi}, \bar{\chi}\}$, and $\bar{\chi} = 0.2$. The violet area corresponding to $\lambda = 0.2$, and the blue one corresponding to $\lambda = 0.4$, are the domains in which the different random samples may fall. They have been obtained with 10^4 independent samples for each value N of the length of the chain.

pens in the Heisenberg case [5]. On the other hand, at fixed λ , the end-to-end concurrence $C_{1,N}$ as a function of the size N of the chain converges very rapidly to its thermodynamic-limit saturation value:

$$C_{1,\infty} = 2 \max \left\{ 0, \frac{1}{2} - \lambda^2 + \frac{\lambda^4}{4} \right\}. \quad (14)$$

Next, it is important to verify that the phenomenon of strong end to end entanglement survives in the presence of disorder. Indeed, in Fig. 2 we represent the behavior of the end-to-end entanglement for different sample realizations of the following Hamiltonian with disordered

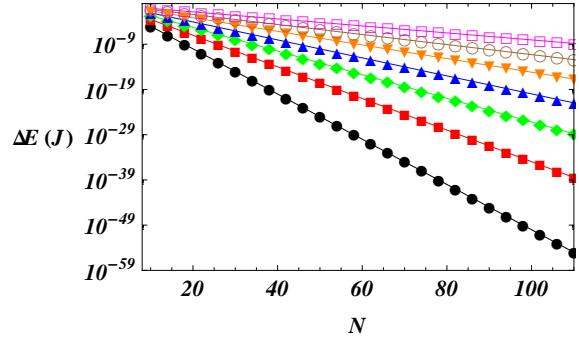


Figure 3: Energy Gap $\Delta E(J)$ between the ground and the first excited state, in units of the coupling energy J , for the 1-D XX spin model with alternating couplings described by the Hamiltonian Eq. (13), plotted as a function of the length N of the chain for different values of the weak coupling λ . From top to bottom: magenta empty squares: $\lambda = 0.7$; brown empty circles: $\lambda = 0.6$; orange inverted triangles: $\lambda = 0.5$; blue triangles: $\lambda = 0.4$; green diamonds: $\lambda = 0.3$; red full squares: $\lambda = 0.2$; black full circles: $\lambda = 0.1$.

couplings:

$$H = \frac{J}{2} \sum_{i=1}^{N-1} [(1+\lambda) + (-1)^i(1-\lambda)](1+\chi_i) (S_i^x S_{i+1}^x + S_i^y S_{i+1}^y), \quad (15)$$

where χ_i is a random variable uniformly distributed in the interval $\{-\bar{\chi}, \bar{\chi}\}$. As we may note, the presence of noise affects bi-directionally the entanglement properties of the system, and the end to end concurrence is non-vanishing even in the presence of a noise with a relative weight of 20%. For nearly half of the samples, noise increases the end to end concurrence. Moreover, Fig. 2 shows that the stronger the end-to-end entanglement without noise, the weaker the relative effect of the noise.

It would then seem that in order to obtain a physical system with strong LDE it should be sufficient to engineer some concrete device that in appropriate limits simulates/realizes an XX spin chain with alternating weak and strong couplings. Unfortunately, this is not the case in realistic situations. As shown in Fig. 3, the phenomenon of perfect LDE is strictly associated to an energy gap between ground and first excited states that vanishes exponentially fast as a function of the length of the chain. Therefore, as soon as the system is at temperatures comparable with the gap ΔE , the equilibrium Gibbs state results in an incoherent superposition of singlet and triplet states in which the LDE vanishes [6, 7]. Consequently, in order to realize a nonvanishing entanglement between the two end points, even in short chains, it would be necessary to reach temperatures fantastically close to absolute zero, something that is well beyond reach in any foreseeable future, and in any case of no use for practical applications.

One might still consider realizing the request of perfect LDE by looking at modifications or alternatives to

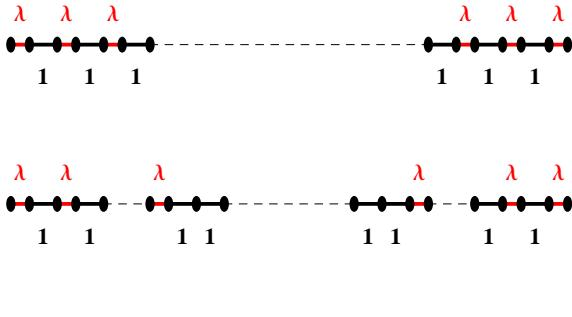


Figure 4: Schematic drawing of XX spin chains endowed with perfect LDE in the GS. Upper drawing: Model Eq.(13), with alternating weak ($\lambda < 1$) and strong couplings along the entire chain. Lower drawing: Model Eq.(16), with left and right end regions of alternating weak and strong couplings and a central (bulk) region of uniform strong couplings.

the pattern of perfectly alternating weak and strong couplings. Such a pattern has been introduced with the aim of suppressing the formation of sizeable entanglement between the end points and the remaining spins of the lattice. However, it is quite clear that this goal can be achieved considering different spatial interaction patterns that have the effect of isolating the bulk of the chain from the end points. This observation motivates the introduction of the following class of Hamiltonians:

$$H = \frac{J}{2} \left[\sum_{i=1}^{\tilde{N}-1} [(1+\lambda) + (-1)^i(1-\lambda)] (S_i^x S_{i+1}^x + S_i^y S_{i+1}^y) + \sum_{i=\tilde{N}}^{N-\tilde{N}-1} 2 (S_i^x S_{i+1}^x + S_i^y S_{i+1}^y) + \sum_{i=N-\tilde{N}}^{N-1} [(1+\lambda) + (-1)^i(1-\lambda)] (S_i^x S_{i+1}^x + S_i^y S_{i+1}^y) \right]. \quad (16)$$

Models Eq.(13) and Eq.(16) with their spatial patterns of site-dependent couplings are sketched pictorially in Fig. 4. The choice of the spatial pattern of the couplings that characterizes model Eq.(13) allows to preserve perfect LDE between the end points of the XX spin chain, at the same time drastically increasing the energy gap between the GS and the first excited states. In practice, it amounts to replace in the bulk of the chain, i.e. between a reference \tilde{N} -th spin and the $N - \tilde{N}$ -th one, the alternating pattern of weak and strong couplings with a uniform nearest-neighbor interaction. The results for the end-to-end entanglement as a function of the length of the chain, for different values of λ and at a fixed value of the ratio \tilde{N}/N are reported in Fig. 5. In the thermodynamic limit, the model described by Eq. (16) exhibits a LDE behaviour analogous to that of the model with fully alternating weak and strong couplings described by Eq.

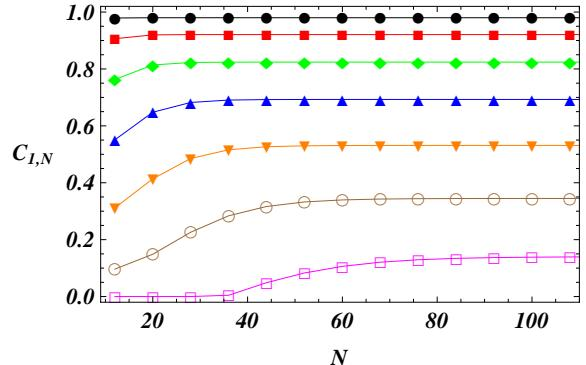


Figure 5: End-to-end concurrence $C_{1,N}$ for an XX spin chain with alternating couplings and a central region with uniform interactions, described by the Hamiltonian Eq.(16), plotted as a function of the length N of the chain, for different values of the weak coupling λ and a fixed value of the ratio $\tilde{N}/N = 1/4$. From bottom to top: magenta empty squares: $\lambda = 0.7$; brown empty circles: $\lambda = 0.6$; orange inverted triangles: $\lambda = 0.5$; blue triangles: $\lambda = 0.4$; green diamonds: $\lambda = 0.3$; red full squares: $\lambda = 0.2$; black full circles: $\lambda = 0.1$.

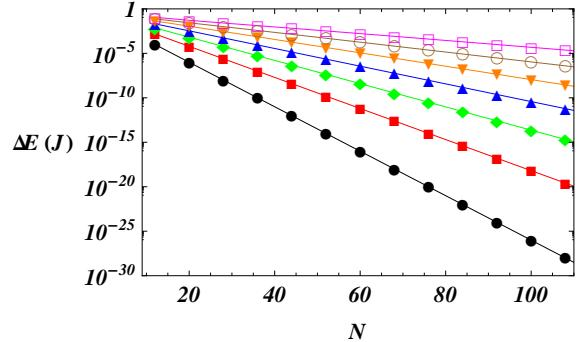


Figure 6: Energy gap, in units of the coupling energy J , between the ground and the first excited state for an XX spin chain with alternating couplings and a central region with uniform interactions, described by the Hamiltonian Eq.(16). The gap $\Delta E(J)$ is plotted as a function of the length N of the chain, for different values of the weak coupling λ and at a fixed value of the ratio $\tilde{N}/N = 1/4$. From top to bottom: magenta empty squares: $\lambda = 0.7$; brown empty circles: $\lambda = 0.6$; orange inverted triangles: $\lambda = 0.5$; blue triangles: $\lambda = 0.4$; green diamonds: $\lambda = 0.3$; red full squares: $\lambda = 0.2$; black full circles: $\lambda = 0.1$.

(13), when the size of the chain is increased at a fixed, constant value of the ratio \tilde{N}/N . The only difference, as can be seen by comparing Fig. 1 with Fig. 5, is that in the second case the end-to-end concurrence reaches the saturation value more slowly, with a speed that decreases when decreasing the ratio \tilde{N}/N . While the essential features of the LDE behaviour are shared also by the modified model with uniform central interactions, the behaviour of the energy gap between the ground and the first excited states is instead strongly affected, as shown in Fig. 6. As we can see from Fig. 6, the energy gap again

decreases as the length of the chain is increased, as in the previous case, and it attains values that forbid possible experimental implementations of LDE at finite temperature (although higher than the corresponding ones for the model with perfectly alternating couplings). Comparing Fig. 6 with Fig. 3 and taking into account that in the present case $\tilde{N} = N/4$ the behavior of the energy gap does not depend on the total length N of the chain, but rather only on the length $2\tilde{N} = N/2$ of that part of the chain characterized by alternating pairings. This dependence of the energy gap on the length of that part of the chain endowed with alternate couplings is confirmed by the analysis of systems defined at different values of \tilde{N} . This fact suggests to investigate further possibilities. Indeed, one may think of bringing the modification implemented in Eq.(16) to the extreme, in order to realize non negligible values of LDE at small, but experimentally feasible temperatures.

B. Quasi Long Distance Entanglement (QLDE)

As we have seen at the end of the previous subsection, reducing the portion of an XX chain with alternating patterns of interaction does not reduce the entanglement shared by the end points and increases by several orders of magnitude the energy gap between the ground and the first excited states, yet, unfortunately, it does not allow LDE to survive except at unrealistically low temperatures. Therefore, in order to realize a nonvanishing LDE at low, but realistically attainable temperatures, we consider taking the limit of Eq.(16) to a model with uniform nearest-neighbor interactions for all pairs of spins but for the two end-points, that are connected to the rest of the chain with a weak bond. Indeed, spin systems allowing for strong end-to-end correlations should be characterized by interactions between the end points and their nearest neighbors that are always smaller than the interactions in the bulk of the chain. Otherwise, if the system does not meet this criterion, the end points would become strongly entangled with their neighbors, excluding, due to the monogamy constraints [27], the possibility of LDE. Hence, we consider an open XX spin chain formed by $N - 2$ spins with uniform coupling strengths, plus two weakly interacting probes placed at the two end points. Such a model is described by the Hamiltonian

$$H = J \sum_{i=2}^{N-2} [S_i^x S_{i+1}^x + S_i^y S_{i+1}^y] + J\lambda (S_1^x S_2^x + S_1^y S_2^y + S_{N-1}^x S_N^x + S_{N-1}^y S_N^y), \quad (17)$$

where $0 < \lambda < 1$. The evolution of the end-to-end concurrence shared by the end points as a function of the length of the chain for different values of the weak coupling λ is reported in Fig.7. At variance with what occurred in the models with patterns of alternating couplings studied in the previous subsection, in the case of models with uniform bulk interactions and weak end

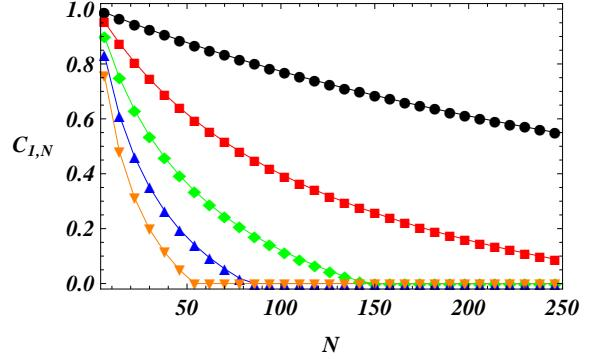


Figure 7: End-to-end concurrence $C_{1,N}$ for an XX spin chain with uniform bulk couplings and two weak end probes described by the Hamiltonian Eq.(17), plotted as a function of the length N of the chain for different values of the weak coupling λ . From bottom to top: orange inverted triangles: $\lambda = 0.2$; blue triangles: $\lambda = 0.16$; green diamonds: $\lambda = 0.12$; red full squares: $\lambda = 0.08$; black full circles: $\lambda = 0.04$.

probes the GS end-to-end entanglement is sensitive to the size of the chain. It decreases slowly as the length of the chain grows and vanishes at a critical value of the length, which depends on the value of the weak coupling λ . This behavior of the GS end-to-end entanglement is due to the fact that the region responsible of preventing the formation of quantum correlations between the end points and the bulk of the chain is fixed at two lattice spacings, and does not grow as the length of the chain is increased. However, by choosing sufficiently small values of the weak coupling λ , it is always possible to realize a GS with nonvanishing LDE in chains of arbitrary finite length. Hence it is natural to name this behaviour as quasi LDE (QLDE), a phenomenon that differs from perfect LDE, as the latter occurs only when the system admits a non vanishing GS end-to-end entanglement that attains its maximum (saturation) value in the thermodynamic limit.

In addition to the QLDE nature of the end-to-end entanglement in the GS, models with weak end bonds possess an energy gap between the GS and the first excited states that exhibits a very different behavior compared to the case of models characterized by LDE. As one can see from Fig. 8, the energy gap does not exhibit an exponential decay with the size of the chain as in the cases of Fig. 3 and Fig. 6. This fact, together with the possibility to choose appropriately the value of λ to ensure a non vanishing QLDE shared by the end points in chains of arbitrary finite length, opens the possibility for the experimental realization of QLDE at low but realistically achievable temperatures with concrete physical systems engineered in configurations suitable for the realization/simulation of model Eq.(17).

Even if the models introduced in the previous subsection and the one described by Eq. (17) show different behaviors of the end to end entanglement, they share the property that it is robust in the presence of noise. Indeed,

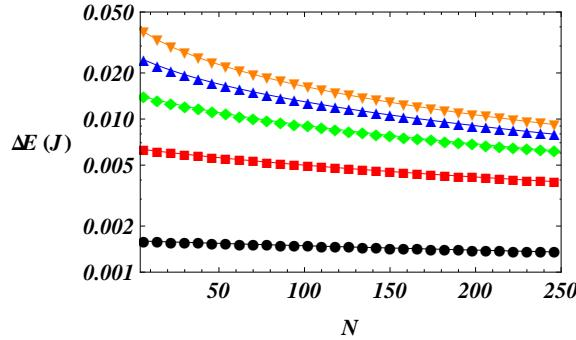


Figure 8: Energy Gap $\Delta E(J)$, in units of the coupling energy J , between the GS and the first excited states for an XX spin chain with weak end probes, described by the Hamiltonian Eq.(17), plotted as a function of the length N of the chain for different values of the weak coupling λ . From top to bottom: orange inverted triangles: $\lambda = 0.2$; blue triangles: $\lambda = 0.16$; green diamonds: $\lambda = 0.12$; red full squares: $\lambda = 0.08$; black full circles: $\lambda = 0.04$.

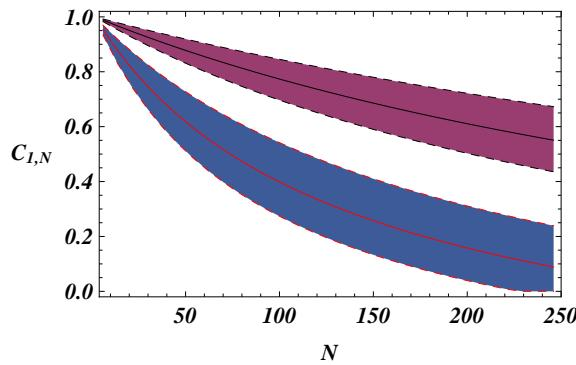


Figure 9: End-to-end entanglement as a function of the length of the chain for the model with disordered couplings described by Eq. (18) where χ_i is a random variable uniformly distributed in the interval $\{-\bar{\chi}, \bar{\chi}\}$ with $\bar{\chi} = 0.2$. The violet area corresponding to $\lambda = 0.2$, and the blue one corresponding to $\lambda = 0.4$, are the domains in which the different random samples may fall. They have been obtained with 10^4 independent samples for each value N of the length of the chain.

Fig. 9 displays the end-to-end entanglement for different realizations of the model with disordered couplings described by the following Hamiltonian:

$$H = J \sum_{i=2}^{N-2} \chi_i [S_i^x S_{i+1}^x + S_i^y S_{i+1}^y] + J(\lambda + \chi_1)(S_1^x S_2^x + S_1^y S_2^y) + J(\lambda + \chi_{N-1})(S_{N-1}^x S_N^x + S_{N-1}^y S_N^y) , \quad (18)$$

where χ_i is a random variable uniformly distributed in the interval $\{-\bar{\chi}, \bar{\chi}\}$. As with models endowed with perfect LDE, also in the case of QLDE the presence of noise affects the end to end concurrence bi-directionally, and the entanglement remains nonvanishing even when the relative weight of the noise is up to 20%. Also in the

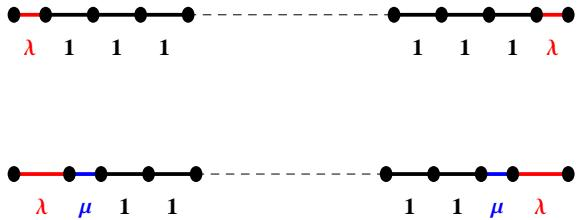


Figure 10: Schematic drawing of XX spin chains endowed with QLDE in the GS. Upper drawing: Model Eq.(17), with weak end bonds $\lambda < 1$ and uniform unit couplings in the bulk. Lower drawing: $\lambda-\mu$ model Eq.(19), with weak end bonds $\lambda < 1$, strong near-end bonds $\mu > 1$, and uniform unit couplings in the bulk.

case of models associated to QLDE, about half of the random sample realizations happen to increase the value of the concurrence between the end points. Moreover, the disruptive effect of noise is strongly reduced for large values of the end-to-end entanglement.

The role played by the two weak interactions in the model Eq.(17) is to force the second ($N-1$ -th) spin of the chain to get heavily entangled with the third ($N-2$ -th) spin, thus forcing the first and last spins of the chain, due to entanglement monogamy and the fact that this configuration is energetically favorable, to develop a nonvanishing quantum correlation in the GS. This effect can be enhanced further by increasing the interaction between the second and the third spin, and correspondingly between the $N-1$ -th and the $N-2$ -th, well above the reference value between neighboring spins in the bulk of the chain. In this case the model Hamiltonian reads:

$$H = J \sum_{i=3}^{N-3} [S_i^x S_{i+1}^x + S_i^y S_{i+1}^y] + \lambda (S_1^x S_2^x + S_1^y S_2^y + S_{N-1}^x S_N^x + S_{N-1}^y S_N^y) + \mu (S_2^x S_3^x + S_2^y S_3^y + S_{N-2}^x S_{N-1}^x + S_{N-2}^y S_{N-1}^y) . \quad (19)$$

Models Eq.(17) and Eq.(19) with their spatial patterns of site-dependent couplings are sketched pictorially in Fig. 10. In Eq.(19) we have $\lambda < 1$ and $\mu > 1$, so that λJ (weak end bond) $< J$ (uniform bulk interaction) $< \mu J$ (strong near-end bond). The increased efficiency granted by model Eq.(19) for the process of creating a nonvanishing QLDE between the two end points of the chain can be appreciated in Fig. 11, where the model (17) with simple weak end bonds $\lambda = 0.1$, $\mu = 1$, is compared with model (19) with the same value of λ and different values of the strong near end bonds $\mu > 1$. In the following, Hamiltonians (17) realizing simple QLDE in the GS will be referred to as λ models, while Hamiltonians (19) that realize enhanced QLDE in the GS will be referred to as $\lambda-\mu$ models. It is not surprising that the

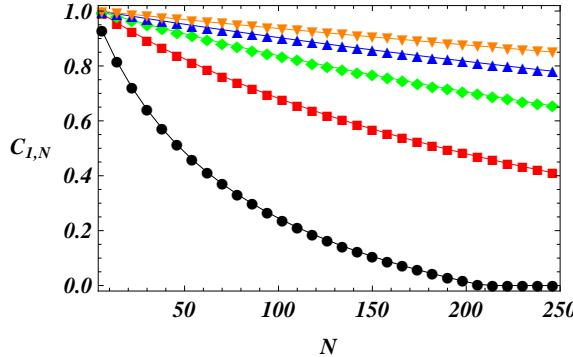


Figure 11: End-to-end concurrence $C_{1,N}$ for the $\lambda-\mu$ spin chain described by Hamiltonian Eq.(19), plotted as a function of the length N of the chain, for a fixed value of the weak coupling $\lambda = 0.1$, and different values of the strong coupling μ . From top down: orange inverted triangles: $\mu = 5$; blue triangles: $\mu = 4$; green diamonds: $\mu = 3$; red full squares $\mu = 2$. The lowest-lying line (black full circles) is the one with $\mu = 1$, corresponding to the λ model Eq.(17), and is drawn for comparison.

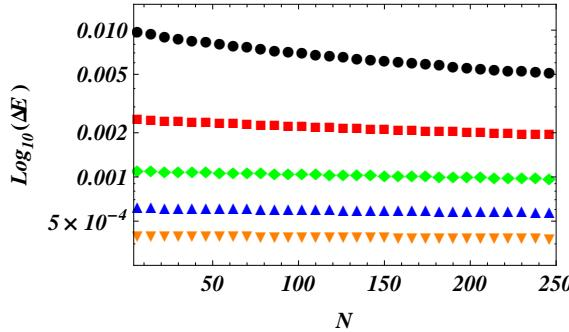


Figure 12: Energy Gap $\Delta E(J)$ (in logarithmic scale), in units of the uniform bulk coupling J , between the GS and the first excited states for the $\lambda-\mu$ spin chain described by Hamiltonian Eq.(19), plotted as a function of the length N of the chain, for a fixed value of the weak coupling $\lambda = 0.1$, and different values of the strong coupling μ . From bottom up: orange inverted triangles: $\mu = 5$; blue triangles: $\mu = 4$; green diamonds: $\mu = 3$; red full squares $\mu = 2$. The line with $\mu = 1$ (black full circles) corresponds to the λ model Eq.(17), and is drawn for comparison.

strong enhancement brought by the $\lambda-\mu$ model to the QLDE that can be accommodated in the GS is obtained at the cost of a (relatively moderate) trade-off with the behaviour of the energy gap. In Fig. 12 we have compared the behaviour of the energy gap, as a function of the size of the system, for the λ model and various $\lambda-\mu$ models with the same value of λ and different values of μ . At this point, the question naturally arises of optimizing the parameters of the Hamiltonian in order to single out the maximum possible value of the QLDE compatible with an energy gap sufficiently large to warrant a concrete physical realizability at finite temperature. Obviously, the process of optimization of the Hamiltonian

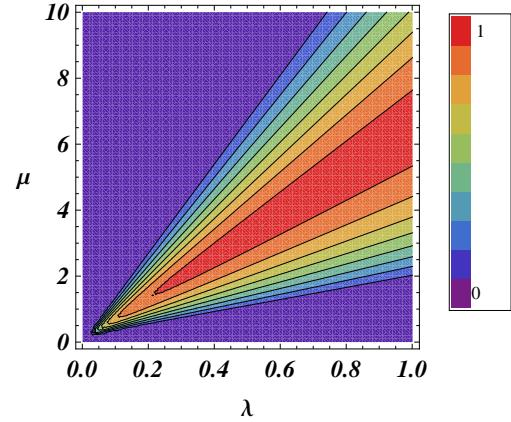


Figure 13: Two-dimensional contour plot of the end-to-end concurrence $C_{1,N}$ as a function of the weak and strong couplings λ and μ , for a 1-D $\lambda-\mu$ spin model (19) on an open linear chain of $N = 10$ spins at a reduced temperature $T/J = 0.05$. The color map relative to the values of the concurrence is reported on the left. Values vary from 0 (violet) to 1 (red).

parameters does not provide a unique general answer. Rather, the results will vary, depending on the length of the chain that one wants/needs to consider as well as on the minimum working temperature that is fixed by the external experimental conditions. In the following we will always consider the models of enhanced QLDE described by Hamiltonian (19), that for $\mu = 1$ reduce to the models (17) of simple QLDE. A typical result of the optimization process for a $\lambda-\mu$ spin chain of finite length is shown in Fig. 13 in the case $N = 10$. It is important to notice that too high values of μ and/or too low values of λ , contrary to naive intuition do not help, because they lead either to an effective separation of the end points from the rest of the chain and/or to a much too small energy gap compared to the energy amplitude of thermal excitations. In both cases, the associated QLDE vanishes. Moreover, the fact that very large values of the end-to-end entanglement are always associated with small energy gaps implies, as the figure shows, that the optimization process is never trivial (especially in determining the regions of matching values for the couplings), and therefore it represents a key point in the discussion of realistic physical systems able to simulate/realize models endowed with QLDE, a subject that we investigate in the following sections.

As with the other cases considered previously, also the $\lambda-\mu$ model is robust against noise affecting the coupling amplitudes. This resilience is shown in Fig. 14, displaying the end-to-end entanglement for different realizations of the model with disordered couplings described by the

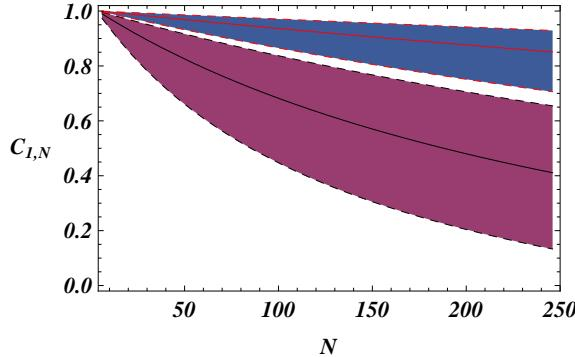


Figure 14: End-to-end entanglement as a function of the length of the chain for the model with disordered couplings described by Eq. (20) where χ_i is a random variable uniformly distributed in the interval $\{-\bar{\chi}, \bar{\chi}\}$ with $\bar{\chi} = 0.2$. The violet area, corresponding to $\lambda = 0.1$ and $\mu = 2.0$ and the blue area, corresponding to $\lambda = 0.1$ and $\mu = 5.0$, are the domains in which the different random samples may fall. They have been obtained with 10^4 independent samples for each value of the length N of the chain.

Hamiltonian:

$$\begin{aligned} H = & J \sum_{i=3}^{N-3} \chi_i [S_i^x S_{i+1}^x + S_i^y S_{i+1}^y] \\ & + \lambda \chi_1 (S_1^x S_2^x + S_1^y S_2^y) \\ & + \lambda \chi_{N-1} (S_{N-1}^x S_N^x + S_{N-1}^y S_N^y), \\ & + \mu \chi_2 (S_2^x S_3^x + S_2^y S_3^y) \\ & + \mu \chi_{N-2} (S_{N-2}^x S_{N-1}^x + S_{N-2}^y S_{N-1}^y). \end{aligned} \quad (20)$$

Here, as in the previous cases, χ_i is a random variable uniformly distributed in the interval $\{-\bar{\chi}, \bar{\chi}\}$.

IV. END-TO-END ENTANGLEMENT IN OPTICAL LATTICES

Until now we have analyzed in some detail the question of identifying specific instances of open XX spin chains with different patterns of site-dependent interactions that possess GSs endowed with large values of the entanglement shared by the end points and an energy gap compatible with physical realizations at finite temperature. Here and in the following we investigate concrete instances of atomic and quantum optical systems that may allow the experimental demonstration of LDE and QLDE.

We first consider systems of ultracold neutral atoms loaded on a one-dimensional optical lattice generated by interfering laser beams [9]. The dynamics of such systems is usually well described, depending on the nature of the atoms present in the ensemble, by a Bose-Hubbard model [28] or by a Fermionic Hubbard model, or by mixtures of atoms of different species, such as Bose-Bose [29], Fermi-Fermi [30], and Bose-Fermi mixtures [31]. Regardless of the specific cases realized, the parameters in the

various Hamiltonians can be easily controlled by tuning both the intensity and the frequency of the laser beams. This fact, i.e. that all the Hamiltonian parameters can be manipulated and modified with a high degree of control, makes optical lattices of particular interest for the simulation/realization of models of interacting quantum systems. The mapping of Hubbard-type models into XX spin models, in appropriate regimes of the parameters, was originally discussed in the fundamental work of Fisher *et al.* [32] where the Bose-Hubbard model was introduced. In recent years, several works have been dedicated to the simulation of spin models using Hubbard Hamiltonians realized in optical lattices. However, in most of these works the spin-spin interactions are usually taken to be either uniform [12, 13] or completely random [14].

Let us consider a 1-D optical chain loaded with single-species ultracold bosonic atoms. The system is described by the 1-D Bose-Hubbard Hamiltonian [28] that can be written as

$$H = \frac{U}{2} \sum_{i=1}^N n_i (n_i - 1) - t \sum_{i=1}^{N-1} (b_i^\dagger b_{i+1} + h.c.) , \quad (21)$$

where b_i^\dagger (b_i) is the creation (annihilation) operator of a bosonic atom at the i -th site of the chain, $n_i = b_i^\dagger b_i$ is the number operator at site i , and N is the number of sites in the chain. The parameter U denotes the strength of the local on-site repulsion, while t is the hopping amplitude between adjacent sites. These Hamiltonian parameters depend on the quantities characterizing the external periodic optical field, taking into account only the lowest vibrational states for every minimum of the periodic potential [28].

The simplest approach to simulate XX spin models starting with the bosonic Hubbard Hamiltonian Eq.(21) relies on the fact that the local Fock states with either one or no particle per site differ from all other local Fock states in that they are the only two local levels whose energy is not dependent on the repulsion. Therefore, in the strong interaction regime ($U \gg t$), they are automatically separated from the others, and hence they can play the role local spin-1/2 states. In the framework of this approximation, the hopping term is naturally mapped in an interaction of the XX type with an amplitude equal to two times the hopping amplitude. However, in an optical lattice, the hopping amplitude between adjacent sites, depends both on the frequency and the intensity of the lasers that are quantities common to each site. Hence, the interaction couplings between adjacent spins in the ensuing XX model are site-independent.

However, site-dependent spin-spin couplings can be easily engineered by introducing local fields on properly selected sites of the lattice. Consider a local field on a given site, say the k -th one, whose amplitude is larger than the hopping amplitudes but weaker than the on-site repulsion U . In this situation occupation of the on-site single-particle Fock state is energetically unfavorable.

Therefore, if an atom in $k+1$ -th or in $k-1$ -th site hops onto the k -th site, it is immediately pushed away. This mechanism realizes either a self-interaction at site k or an effective interaction between the $k+1$ -th and the $k-1$ -th site. This simple reasoning can be put in a quantitative form resorting to degenerate perturbation theory in powers of the hopping amplitude. Let $k-1$, k , and $k+1$ be three adjacent sites, let $\varepsilon_k \neq 0$ the local field at site k , and such that $t \ll \varepsilon_k \ll U$. In second-order perturbation, discarding all the excited states with energy proportional to U and ε_k , each pair term in Eq.(21) maps into the following spin-spin interaction:

$$H_k = -\frac{2t^2}{\varepsilon_k} (S_{k-1}^x S_{k+1}^x + S_{k-1}^y S_{k+1}^y) - \frac{t^2}{\varepsilon_k} \left(S_{k-1}^z + \frac{1}{2} \right)^2 - \frac{t^2}{\varepsilon_k} \left(S_{k+1}^z + \frac{1}{2} \right)^2 . \quad (22)$$

It is important to note that in these spin-spin interaction terms the dependence on the k -th site is removed. Hence, the introduction of site-dependent spin-spin interaction strengths is associated to a reduction of the sites of the optical lattice. Eq.(22) is the basic ingredient in the realization of XX spin chains with site-dependent interactions and nonvanishing end-to-end entanglement. The successive task is to determine suitably engineered optical lattices with the appropriate local field dynamics. For instance, one possible way to realize the XX spin model with alternating weak and strong couplings Eq.13 is to introduce an optical super-lattice potential obtained through the interference of two sets of laser beams of different amplitude strengths. The set of stronger beams realizes the lattice structure while the set of weaker ones realizes and modulates the presence of a local field at each lattice site. If, for instance, the set of weak beams is tuned at a wavelength three times as large as that of the set of strong ones, one realizes a system in which every site over three is characterized by a strong local field, while the remaining two sites experience a practically vanishing local field, as schematically illustrate in Fig. 15. Resorting to degenerate second-order perturbation theory in powers of t , and taking into account Eq.(22), the optical lattices Hamiltonian is mapped in the spin Hamiltonian

$$H = -t \sum_{i=1}^{N'-1} \left[\left(1 + \frac{t}{\varepsilon} \right) + (-1)^i \left(1 - \frac{t}{\varepsilon} \right) \right] \times (S_i^x S_{i+1}^x + S_i^y S_{i+1}^y) - \frac{t^2}{\varepsilon} \sum_{i=1}^{N'} \left(S_i^z + \frac{1}{2} \right)^2 , \quad (23)$$

where $\varepsilon > t$ is the maximum amplitude of the local field, and $N' = 2N/3$ is the number of spins in the chain that, as already noticed, does not coincide with the number of sites in the physical optical lattice chain. The last sum of terms represents an overall energy offset that can always be reabsorbed in the definition of the zero of the energy and has no dynamical effect. Fixing the total

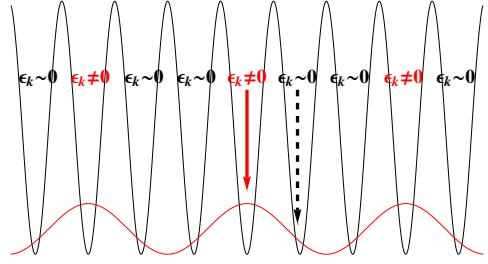


Figure 15: Scheme of the optical super-lattice potential obtained by combining two appropriate sets of stationary laser beams. It realizes an effective XX spin chain with alternating weak and strong interactions that allows for LDE between the two end points. The first set of laser beams generates an optical potential (black line) that realize an optical lattice. On the contrary, the weaker optical potential of the second sets, represented by the red line, creates a local field at each site of the optical lattice. The local field is strongly enhanced on every site over three.

magnetization at 0, corresponds to fixing the number of atoms in the optical lattice at $n = N'/2 = N/3$. In this case we obtain that in the strong interaction regime the optical super-lattice simulates the 1-D XX spin chain with alternating weak and strong couplings Eq.13, exactly with $\lambda = t/\varepsilon$. It is important to verify the soundness of the theoretical mapping, obtained in second-order perturbation theory, by direct exact numerical comparison between the end-to-end entanglement properties of the spin model Eq.13 and of the original bosonic system. In Fig. 16 we report the end-to-end entanglement in the GS of a system of ultracold bosonic atoms loaded on the above-described optical super-lattice, with $N = 12$ sites and $n = N/3 = 4$ atoms, corresponding, according to the our previous analysis, to a 1-D XX spin chain with $N' = 2N/3 = 8$ sites with alternating weak and strong couplings. As measures of entanglement, we consider the concurrence [22] and the logarithmic negativity [33]. The concurrence quantifies the GS entanglement between the two end points seen as effective spins, obtained by tracing out all Fock states but the empty state and the state with single-atom occupation. The logarithmic negativity is used to measure the actual GS entanglement of the full bosonic system between the two end sites of the optical super-lattice. Fig. 16 shows that for small values of the on-site repulsion U there is no end-to-end entanglement regardless of the value of the local field ε . Viceversa, in the strong interaction regime the system develops a sizeable end-to-end entanglement that always approximates very closely the end-to-end entanglement of the XX spin chain with alternating weak and strong couplings, proving that appropriate optical lattice or super-lattice structures can simulate/realize efficiently XX spin chains with LDE entanglement. An exception is constituted by the limiting case $\varepsilon = t$. In this situation the strong local field condition $\varepsilon > t$ is violated, $\lambda = 1$ in the correspond-

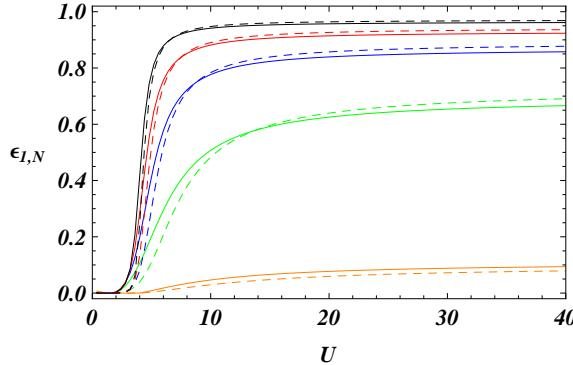


Figure 16: End-to-end entanglement in the GS of a super-lattice system of $N = 12$ sites and $n = 4$ atoms, with strong local field ε on $2 - nd$, $5 - th$, $8 - th$, and $11 - th$ site, plotted as a function of the on-site repulsion U in units of the hopping amplitude t . The dashed lines represent the logarithmic negativity, measuring the end-to-end entanglement in the original Bose-Hubbard atomic system, while the solid lines stand for the concurrence, that measures the end-to-end entanglement in the effective XX spin model with alternating weak and strong couplings. The different curves correspond to different values of the strong local field ε . From bottom up: orange: $\varepsilon = t$; green: $\varepsilon = 3t$; blue: $\varepsilon = 5t$; red: $\varepsilon = 7t$; black: $\varepsilon = 10t$.

ing spin Hamiltonian, and thus the end-to-end spin-spin concurrence vanishes, while the end-to-end logarithmic negativity in the GS of the original optical super-lattice system is definitely nonvanishing.

We now turn to the question of simulating spin models with QLDE rather than pure LDE. One problem in simulating the Hamiltonians described in Subsection III B with atomic systems in optical potential structures is that QLDE models do not have a periodic pattern of site-dependent interactions and thus are difficult to approximate with super-lattices, as done for LDE models. Spin models with QLDE structures can be simulated by addressing the degrees of freedom of the individual lattice sites with pre-selection techniques that have recently been discussed for different purposes [34], [35]. If these methods, or similar ones, could be implemented successfully in realistic experimental conditions, it would be possible to realize optical-lattice structures such that only few pre-selected sites are affected by a nonvanishing local field. Consider the following Bose-Hubbard Hamiltonian

$$H = \frac{U}{2} \sum_{i=1}^N n_i(n_i - 1) - t \sum_{i=1}^{N-1} (b_i^\dagger b_{i+1} + h.c.) + \varepsilon(n_2 + n_{N-1}). \quad (24)$$

The presence of a local field ε at the second and $N - 1$ -th sites allows to simulate, when $t < \varepsilon < U$, the XX spin model with weak end probes described by Eq.(17). In Fig.(17) we report the GS end-to-end entanglement for the Hamiltonian Eq. (24) defined on an optical lattice of $N = 10$ sites and loaded with $n = 4$ bosonic atoms, and compare it with the GS end-to-end entanglement of

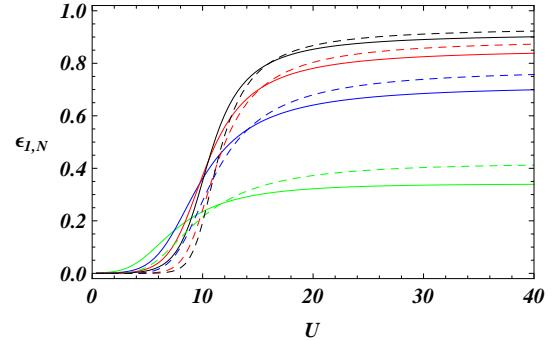


Figure 17: End-to-end entanglement in the GS of the Bose-Hubbard Hamiltonian Eq. (24), defined on an optical lattice of $N = 10$ sites with strong local field on the $2 - nd$ and on the $9 - th$ site, plotted as a function of the on-site repulsion U in units of the hopping amplitude t . The dashed lines correspond to the logarithmic negativity measuring the end-to-end entanglement in the original Bose-Hubbard atomic system, while the solid lines stand for the concurrence, that measures the end-to-end entanglement in the effective XX spin model with weak end probes. The different curves correspond to different values of the local field ε . From bottom up: green: $\varepsilon = 3t$; blue: $\varepsilon = 6t$; red: $\varepsilon = 9t$; black: $\varepsilon = 12t$.

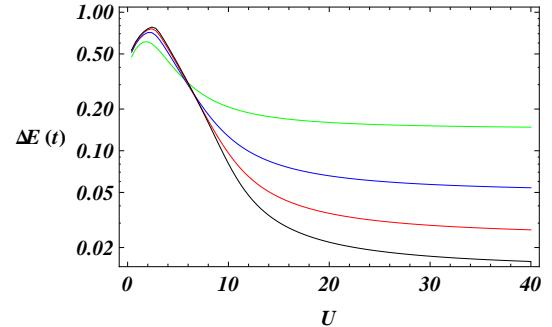


Figure 18: Energy gap between the GS and the first excited states of the Bose-Hubbard Hamiltonian Eq. (24), defined on an optical lattice of $N = 10$ sites with strong local field on the $2 - nd$ and on the $9 - th$ site, plotted as a function of the on-site repulsion U in units of the hopping amplitude t . The different curves correspond to different values of the local field ε . From bottom up: green: $\varepsilon = 3t$; blue: $\varepsilon = 6t$; red: $\varepsilon = 9t$; black: $\varepsilon = 12t$.

an XX model with weak end probes Eq.(17) defined on a chain with 8 spins. We see that the former is an excellent approximation to the latter in the limit of large on-site repulsion U . We have fixed the total number of bosonic atoms to $(N-2)/2$ to satisfy the half-filling condition. This corresponds again to impose a vanishing magnetization in the effective spin chain. In the strong-coupling regime, the value of the end-to-end entanglement grows as the local field ε is increased, as should be expected from the results of the discussion in Subsection III B, taking into account Eq. (22). However, as discussed in the previous section, the significance of simulating/realizing spin models with QLDE using, for in-

stance, optical lattice Hamiltonian structures as the ones described by Eq. (24) is that the energy gap can be sufficiently large to ensure that a nonvanishing end-to-end entanglement is still retained at very low but realistically reachable working temperatures. The two requirements of large values of QLDE and a large energy gap are partly conflicting. The behavior of the energy gap is reported in Fig.18. Comparing Figs.17 and 18 we see that the optimal compromise, that allows to obtain both a sizeable QLDE and a sizeable energy gap, takes place in initial side of the strong-coupling regime, at moderately large values of the on-site repulsion U .

V. END-TO-END ENTANGLEMENT IN ARRAYS OF COUPLED OPTICAL CAVITIES

Recently, hybrid atom-optical systems of coupled cavity arrays (CCAs) have been intensively studied in relation to their ability to simulate collective phenomena typical of strongly correlated systems [15, 16, 17, 18, 19]. In the present section we will discuss in detail some recent findings [8] about the possibility of exploiting appropriately engineered arrays of coupled optical cavities to realize XX open spin chains sustaining LDE or QLDE. Besides the extremely high controllability and the straightforward addressability of single constituents, arrays of coupled cavities also allow in principle a great degree of flexibility in their design and geometry [10]. Therefore, they should be tested as natural candidates for the realization of spatially extended communication networks and scalable computation devices.

Consider a linear CCA with open ends, consisting of N cavities. The dynamics of a single constituent of the array doped with a single two-level atom is well described by the Jaynes-Cummings Hamiltonian [36]

$$H_k = \omega a_k^\dagger a_k + \omega' |e_k\rangle\langle e_k| + g a_k^\dagger |g_k\rangle\langle e_k| + g |e_k\rangle\langle a_k| a_k , \quad (25)$$

where a_k (a_k^\dagger) is the annihilation (creation) operator of photons with energy ω in the k -th cavity, $|g_k\rangle$ and $|e_k\rangle$ are respectively the ground and excited atomic states, separated by the gap ω' , and g is the photon-atom coupling strength. The local Hamiltonian Eq. (25) is immediately diagonalized in the basis of dressed photonic and atomic excitations (polaritons):

$$|\emptyset_k\rangle = |g_k\rangle|0_k\rangle ; \quad (26)$$

$$|n+k\rangle = \cos \theta_n |g_k\rangle|n_k\rangle + \sin \theta_n |e_k\rangle|(n-1)_k\rangle \quad n \geq 1 ;$$

$$|n-k\rangle = \sin \theta_n |g_k\rangle|n_k\rangle - \cos \theta_n |e_k\rangle|(n-1)_k\rangle \quad n \geq 1 ,$$

where θ_n is given by $\tan 2\theta_n = -g\sqrt{n}/\Delta$ and $\Delta = \omega' - \omega$ is the atom-light detuning. Each polariton is characterized by an energy equal to

$$\varepsilon_0 = 0; \quad \varepsilon_{n\pm} = n\omega \pm \sqrt{ng^2 + \Delta^2} . \quad (27)$$

When $\omega = \sqrt{g^2 + \Delta^2}$ the GS of Eq. (25) becomes two-fold degenerate, resulting in a superposition of $|\emptyset_k\rangle$ and

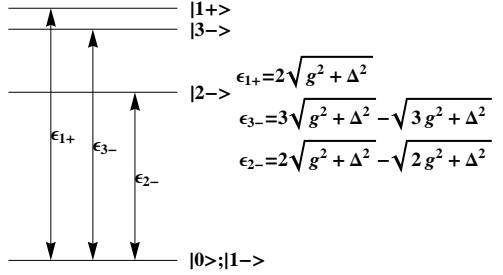


Figure 19: Representation of the energy levels for a cavity with $\omega = \sqrt{g^2 + \Delta^2}$. The GS is two-fold degenerate, and the energy gap ε_{2-} prevents the occupancy of the higher energy levels, thus realizing an effective two-level system.

$|1-k\rangle$, see Fig. 19. If both the atom-cavity interaction energy and the working temperature are small compared to $\varepsilon_{2-} = 2\sqrt{g^2 + \Delta^2} - \sqrt{2g^2 + \Delta^2}$, one may neglect all the local polaritonic states but $|\emptyset_k\rangle$ and $|1-k\rangle$. This situation defines a local two-level system. Adjacent cavities can be easily coupled either by photon hopping or via wave guides of different dielectric and conducting properties. The wave function overlap of two adjacent cavities introduces the associated tunneling elements, so that the total Hamiltonian of the CCA reads:

$$H_{cca} = \sum_k^N H_k - \sum_k^{N-1} J_k (a_k^\dagger a_{k+1} + a_{k+1}^\dagger a_k) . \quad (28)$$

Each hopping amplitude J_k depends strongly on both the geometry of the cavities and the actual overlap between adjacent cavities. If the maximum value among all the couplings $\{J_k\}$ is much smaller than the energy of the first excited state: $\max\{J_k\} \ll \varepsilon_{2-}$, then the total Hamiltonian Eq. (28) can be mapped in a spin-1/2 model of the XX type with site-dependent couplings of the form Eq. (19), where the state $|\emptyset_k\rangle$ ($|1-k\rangle$) plays the role of $|\downarrow_k\rangle$ ($|\uparrow_k\rangle$). The mapping to an open-end $\lambda-\mu$ linear spin chain sustaining QLDE in the GS is then realized, e.g., by simply tuning the distance between the end- and next-to-end sites of the array, as showed in Fig. 20. The $\lambda-\mu$ XX spin chain thus can be realized starting from an equispaced CCA with site-independent nearest-neighbor bulk coupling amplitude J_b , and then engineering appropriately the positions of the $2-nd$ and of the $(N-1)-th$ cavities, that are placed closer to their neighbors in the bulk and farther away from the end points of the array. This shift lowers below unity the reduced coupling between the end points of the array and their next-to-end neighbors ($J_1/J_b = J_{N-1}/J_b = \lambda < 1$), and increases above unity the reduced coupling between the next-to-end sites and their neighbors in the bulk ($J_2/J_b = J_{N-2}/J_b = \mu > 1$), effectively realizing the $\lambda-\mu$ model of QLDE. Obviously, adjusting the hopping rate by spacing the cavities closer to the end points is not the only way to realize the $\lambda-\mu$ model in an array of optical cavities. Indeed, it can be technically rather challenging. An alternative way to tune the inter-cavity

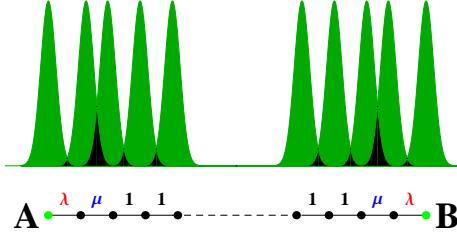


Figure 20: Scheme of an array of coupled optical cavities realizing a $\lambda-\mu$ linear spin chain described in Eq. (19). Dark green: Area covered by the wave functions associated to each site of the array. The two next-to-end sites (light green circles) are symmetrically displaced with respect to a situation of perfectly equispaced sites, and drawn closer to their neighbors in the bulk (black circles). As a consequence, the overlap (black area) between the wave functions of these two cavities and their neighbors in the bulk is larger than the would-be reference (unit) overlap in an equispaced array. At the same time, the overlap between the end sites of the array (red and blue circles) and the next-to-end sites is reduced proportionally compared to an equispaced array.

hopping amplitudes, probably much more feasible with currently available technologies, is to dope the cavities with few-level atoms and use Raman transitions and the atomic Lambda level structures to tune the couplings between two cavities *in situ*, by using external laser drives as described, e.g., in Ref. [19].

In the next section we will discuss the properties of QLDE, realized using CCAs, in connection with the implementation of tasks of quantum information science. In particular, we will discuss how the $\lambda-\mu$ model and the associated GS QLDE can be exploited to realize high-fidelity, long-distance quantum teleportation protocols.

VI. APPLICATIONS: QLDE AND LONG-DISTANCE QUANTUM TELEPORTATION IN CCAS

We now proceed to illustrate that CCAs in the $\lambda-\mu$ configuration allow for long-distance and high-fidelity quantum communication in realistic conditions and at moderately high temperatures. In Fig. 21 we report the fidelity of teleportation F_{max} [24] as a function of the reduced couplings λ and μ for different temperatures. Remarkably, Fig. 21 shows the existence of a rather high *critical* temperature of teleportation for CCAs realizing a $\lambda-\mu$ spin chain. The region of the physical parameters compatible with a nonclassical fidelity $F_{max} > 2/3$ is progressively reduced with increasing temperature, until it disappears at $T_c \approx 0.13J_b$. Similar behaviors are observed for longer CCAs, with T_c slowly decreasing with the length of the array. For instance, for an array of $N = 36$ cavities in the $\lambda-\mu$ configuration, the critical temperature of transition to *bona fide* quantum telepor-

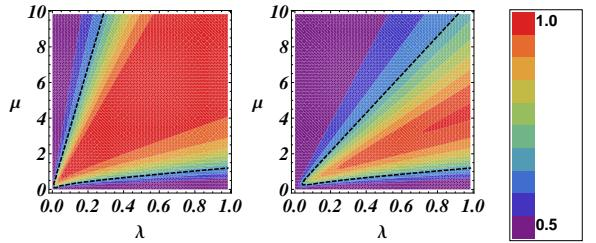


Figure 21: (Color online) Fidelity of teleportation F_{max} in a $\lambda-\mu$ configuration, by exact numerical diagonalization, for a CCA of $N = 12$ cavities as a function of the couplings $\lambda = J_1/J_b$ and $\mu = J_2/J_b$ at different temperatures T/J_b . Left panel: $T/J_b = 0.005$. Right panel: $T/J_b = 0.01$. F_{max} varies between 0.5 (violet) and 1 (red). Horizontal dashed line: Classical threshold $F_{max}^c = 2/3$.

tation is $T_c \approx 0.11J_b$.

A formidable obstacle to the concrete realization of working quantum teleportation devices is performing the projection over a Bell state, in order for the sender to teleport a quantum state faithfully to the receiver. In fact, in the framework of condensed matter devices there hardly exist quantities, easily available in current and foreseeable experiments, that admit as eigenstates any two-qubit Bell states. To avoid this problem different schemes for quantum information transfer have been developed, for instance, for what concerns entanglement transfer, in Ref. [37]. In the following, we will discuss a simple and concrete scheme for long-distance, high-fidelity quantum teleportation in $\lambda-\mu$ CCAs that realizes Bell-state projections indirectly, by matching together free evolutions and local measurements of easily controllable experimental quantities [38, 39, 40]. We first illustrate it in the simplest case of two cavities at zero temperature, with the first cavity accessible by the sender and the second one by the receiver. The sender has access also to a third cavity, the "0" cavity, that is decoupled from the rest of the chain, and stores the state to be teleported $|\varphi\rangle = \alpha|\uparrow_0\rangle + \beta|\downarrow_0\rangle$. The decoupling between the $0 - th$ cavity and the rest of the chain can be achieved removing the degeneracy among $|0\rangle_0$ and $|1\rangle_0$ and taking $|\varepsilon_0 - \varepsilon_1| \gg J_0$. The total system is initially in the state

$$|\Psi(0)\rangle = \frac{1}{\sqrt{2}}(\alpha|\uparrow_0\rangle + \beta|\downarrow_0\rangle)(|\uparrow_1\rangle|\downarrow_2\rangle + |\downarrow_1\rangle|\uparrow_2\rangle). \quad (29)$$

At $t = 0$ the state begins to evolve and if $J_0 \gg J_1$ one has:

$$\begin{aligned} |\Psi(t)\rangle &= \frac{1}{\sqrt{2}}[\alpha|\uparrow_0\rangle|\uparrow_1\rangle|\downarrow_2\rangle + \beta|\downarrow_0\rangle|\downarrow_1\rangle|\uparrow_2\rangle \\ &\quad |\uparrow_0\rangle|\downarrow_1\rangle(\alpha \cos(J_0 t)|\uparrow_2\rangle - i\beta \sin(J_0 t)|\downarrow_2\rangle) \\ &\quad |\downarrow_0\rangle|\uparrow_1\rangle(-i\alpha \sin(J_0 t)|\uparrow_2\rangle + \beta \cos(J_0 t)|\downarrow_2\rangle)]. \end{aligned} \quad (30)$$

If at time $t = \pi/(4J_0)$ Alice measures the local magnetizations (S_0^z, S_1^z) in the first two cavities, she will find with probability 1/2 that the teleported state is the image of $|\varphi\rangle$ under a local rotation. The value 1/2 for the

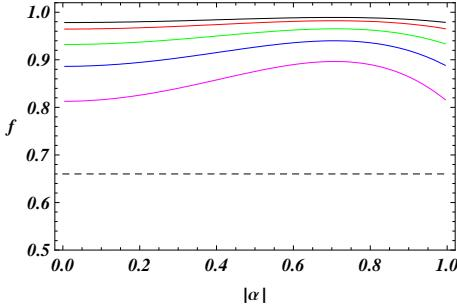


Figure 22: (Color online) Fidelity of teleportation f in a $\lambda\text{-}\mu$ CCA channel of $N = 12$ cavities, for a generic input $|\varphi\rangle = \alpha| \uparrow_0 \rangle + \beta| \downarrow_0 \rangle$, as a function of $|\alpha|$ at different temperatures. Black line: $T = 0.001J_b$; Red line: $T = 0.003J_b$; Green line: $T = 0.004J_b$; Blue line: $T = 0.005J_b$; Magenta line: $T = 0.007J_b$. Here $\lambda = 0.5$, $\mu = 4.0$, and $\nu = 50$. Horizontal dashed line: Classical threshold $f_c = 2/3$.

probability stems from the fact that any simultaneous eigenstate of S_0^z and S_1^z can be obtained with equal probability but one may discard the case in which the total magnetization is equal to ± 1 . Realizing a local rotation of $\pm\pi/2$ around S_2^z , with the sign depending on the result of the measurement that the sender communicates classically to the receiver, the latter recovers the original state $|\varphi\rangle$ with unit fidelity. The simple protocol described above can be immediately extended to $\lambda\text{-}\mu$ CCAs of any size, at finite temperature, and removing the constraint $J_1 \ll J_0$. By resorting again to exact diagonalization, in Fig. 22 we report the behavior of the average fidelity of teleportation f , as a function of $|\alpha|$ of the state $|\varphi\rangle$, in the case of an array of $N = 12$ cavities, with $\nu \equiv J_0/J_b = 50$ and for different temperatures. Also in the non-ideal case the teleportation protocol has probability 1/2 of success. The fidelity depends on the input state, with a maximum for inputs with $|\alpha| = |\beta| = 1/\sqrt{2}$ and a minimum for inputs with $|\alpha| = 0.1$. The fidelity remains above 0.95 for all values of $|\alpha|$ at moderately low temperatures ($T \simeq 10^{-3}J_b$).

VII. CONCLUSIONS AND OUTLOOK

In conclusion, we have introduced some classes of quantum spin models defined on open 1-D lattices that are characterized by non-perturbative GSs with nonvanishing LDE or QLDE. In particular, end-to-end QLDE is found to be strongly resilient to thermal decoherence and can be efficiently achieved with a minimal set of local actions on the end- and near-end couplings in linear open CCAs. We have showed that QLDE-based CCAs allow for a simple quasi-deterministic protocol of long-distance, high-fidelity quantum teleportation that yields a high rate of success without direct Bell measurements and projections over Bell states. In detail, we have studied models of XX quantum spin chains with nearest-neighbor interactions, discussing two types of spatial patterns of

the coupling strengths. In the case of chains with bonds of alternating strengths, we have shown that the exact GS possesses a nonvanishing LDE between the end spins of the chain, independently of the size of the system and asymptotically close to unity (maximal entanglement) in the limit of exact dimerization. This system is therefore perfectly suited for *bona fide* long-distance quantum teleportation with ideal fidelity at zero temperature. However, the limiting maximal values of the fidelity are obtained at the cost of introducing an energy gap above the GS that vanishes exponentially with the size of the system. Therefore, this model is *de facto* useless for efficient quantum teleportation at finite temperature. We have then discussed another class of XX open spin chains with uniform bulk interactions and small end bonds. In this case, we have shown that for sufficiently small values of the end couplings, the GS of the system possesses a sizeable QLDE between the end spins of the chain, that at fixed size of the system is asymptotically close to unity (maximal entanglement) in the limit of vanishingly small end bonds. However, QLDE decreases, albeit slowly, as the size of the system is increased. Models of QLDE can be improved further by introducing strong near-end bonds that enhance the value of the end-to-end entanglement ($\lambda\text{-}\mu$ model). An interesting feature of QLDE models is that the energy gap above the GS vanishes only algebraically, as the first power of the inverse of the size of the system. Therefore, in principle, spin chains endowed with the QLDE property can be exploited as quantum channel for teleportation with nonclassical fidelity at finite temperature.

A relevant issue concerned the behavior of these systems in the presence of disorder. This question is important especially in view of possible experimental implementations in which the couplings can be engineered only within a certain accuracy. Since naturally the effect of disorder is that of localizing eigenstates, we expected LDE to be more robust than QLDE against disorder. In fact, in the LDE scenario the states responsible for the end-to-end entanglement is already localized at the borders whereas localization is only approximate in the QLDE case. This conjecture has in fact been confirmed by thorough exact numerical samplings, that also show that the relative weight of imperfections that can be tolerated by the systems, maintaining large and useful values of LDE and QLDE, is rather high, up to 20%, and more. Moreover, for about always half of the spatial patterns and values of the couplings, disorder can even enhance the end-to-end entanglement. It is at the moment unclear how this picture extends to finite temperature. Another interesting open problem worth further study is to assess the existence and the possible location of a crossover between perfect LDE and *prima facie* QLDE.

Demonstrating experimentally (Q)LDE and (Q)LDE-based efficient long-distance teleportation and state transfer will be a first crucial preliminary test in order to proceed with integrated devices of quantum information science, combining atom-optical systems such as op-

tical lattices or systems of trapped ions with solid-state based systems, such as those of circuit Cavity Quantum Electrodynamics.

Acknowledgments

This work has been realized in the framework of the FP7 STREP Project HIP (Hybrid Information Processing). It is a pleasure to thank Rosario Fazio for some very useful remarks on the implementation of LDE in op-

tical lattices, and with Lorenzo Campos Venuti, Cristian Degli Esposti Boschi, and Marco Roncaglia for discussions. The authors acknowledge financial support from the European Commission of the European Union under the FP7 STREP Project HIP (Hybrid Information Processing), Grant Agreement n. 221889, from MIUR under the FARB funds for the years 2007 and 2008, from INFN under Iniziativa Specifica PG 62, and from CNR-INFN Research Center Coherentia. One of us (F. I.) acknowledges support from the ISI Foundation for Scientific Interchange.

-
- [1] M. A. Nielsen and I. L. Chuang, *Quantum Computation and Quantum Information* (Cambridge University Press, Cambridge, UK, 2000).
 - [2] N. Gisin, G. Ribordy, W. Tittel, and H. Zbinden, Rev. Mod. Phys. **74**, 145 (2002).
 - [3] C. M. Caves and P. D. Drummond, Rev. Mod. Phys. **66**, 481 (1994); J. H. Shapiro and O. Hirota (Eds.), *Quantum Communication, Measurements, and Computing* (Rinton Press, Princeton, N.J., U.S.A., 2003).
 - [4] F. Verstraete, M. Popp, and J. I. Cirac, Phys. Rev. Lett. **92**, 027901 (2004).
 - [5] L. Campos Venuti, C. Degli Esposti Boschi, and M. Roncaglia, Phys. Rev. Lett. **96**, 247206 (2006).
 - [6] L. Campos Venuti, C. Degli Esposti Boschi, and M. Roncaglia, Phys. Rev. Lett. **99**, 060401 (2007).
 - [7] L. Campos Venuti, S. M. Giampaolo, F. Illuminati, and P. Zanardi, Phys. Rev. A **76**, 052328 (2007).
 - [8] S. M. Giampaolo and F. Illuminati, Phys. Rev. A **80**, 050301(R) (2009).
 - [9] I. Bloch, Nature Phys. **1**, 23 (2005).
 - [10] M. J. Hartmann, F. G. S. L. Brandão, and M. B. Plenio, Laser & Photon. Rev. **2**, 527 (2008).
 - [11] A. Sørensen and K. Mølmer, Phys. Rev. Lett. **83**, 2274 (1999).
 - [12] L.-M. Duan, E. Demler, and M. D. Lukin, Phys. Rev. Lett. **91**, 090402 (2003).
 - [13] A. B. Kuklov and B. V. Svistunov, Phys. Rev. Lett. **90**, 100401 (2003).
 - [14] A. Sanpera, A. Kantian, L. Sanchez-Palencia, J. Zakszewski, and M. Lewenstein Phys. Rev. Lett. **93** 040401 (2004).
 - [15] M. J. Hartmann, F. G. S. L. Brandão, and M. B. Plenio, Nature Phys. **2**, 849 (2006).
 - [16] A. D. Greentree, C. Tahan, J. H. Cole, and L. C. L. Hollenberg, Nature Phys. **2**, 856 (2006).
 - [17] D. G. Angelakis, M. F. Santos, and S. Bose, Phys. Rev. A **76**, 031805(R) (2007).
 - [18] D. Rossini and R. Fazio, Phys. Rev. Lett. **99**, 186401 (2007).
 - [19] M. J. Hartmann, F. G. S. L. Brandão, and M. B. Plenio, Phys. Rev. Lett. **99**, 160501 (2007).
 - [20] E. Lieb, T. Schultz, and D. Mattis, Ann. Phys. (N.Y.) **16**, 407 (1961).
 - [21] P. Jordan and E. Wigner, Z. Physik **47**, 631 (1928).
 - [22] W. K. Wootters, Phys. Rev. Lett. **80**, 2245 (1998); S. Hill and W. K. Wootters, Phys. Rev. Lett. **78**, 5022 (1997).
 - [23] L. Amico, A. Osterloh, F. Plastina, R. Fazio and G. M. Palma, Phys. Rev. A **69**, 022304 (2004), P. Zanardi and X. Wang, J. Phys. A, **35**, 7947 (2002).
 - [24] M. Horodecki, P. Horodecki, and R. Horodecki, Phys. Rev. A **60**, 1888 (1999).
 - [25] P. Badziah, M. Horodecki, P. Horodecki, and R. Horodecki, Phys. Rev. A. **62**, 012311 (2000).
 - [26] A. Wojcik, T. Luczak, P. Kurzynski, A. Grudka, T. Gdala, and M. Bednarska, Phys. Rev. A **72**, 034303 (2005).
 - [27] V. Coffman, J. Kundu, and W. K. Wootters, Phys. Rev. A, **61**, 052306 (2000); T. J. Osborne and F. Verstraete, Phys. Rev. Lett. **96**, 220503 (2006).
 - [28] D. Jaksch, C. Bruder J. I. Cirac, C. W. Gardiner, and P. Zoller, Phys. Rev. Lett. **81**, 3108 (1998).
 - [29] P. Buonsante, S. M. Giampaolo, F. Illuminati, V. Penna, and A. Vezzani, Phys. Rev. Lett. **100**, 240402 (2008).
 - [30] M. Iskin and C. A. R. Sa de Melo, Phys. Rev. A **78**, 013607 (2008).
 - [31] F. Illuminati and A. Albus, Phys. Rev. Lett. **93**, 090406 (2004).
 - [32] M. P. A. Fisher, P. B. Weichman, G. Grinstein, D. S. Fisher, Phys. Rev. B **40**, 546 (1989).
 - [33] See, e. g., M. B. Plenio, Phys. Rev. Lett. **95**, 090503 (2005), and references therein.
 - [34] C. Zhang, S. L. Rolston, and S. Das Sarma, Phys. Rev. A **74**, 042316 (2006).
 - [35] J. Cho, Phys. Rev. Lett. **99**, 020502 (2007).
 - [36] E. T. Jaynes and F. W. Cummings, Proc. IEEE **51**, 89 (1963).
 - [37] M. J. Hartmann, M. E. Reuter and M. B. Plenio, New J. Phys. **8**, 94 (2006).
 - [38] S.-B. Zheng, Phys. Rev. A **69**, 064302 (2004).
 - [39] L. Ye and G-C. Guo, Phys. Rev. A **70**, 054303 (2004).
 - [40] W. B. Cardoso, A. T. Avelar, B. Baseia, and N. G. de Almeida, Phys. Rev. A **72**, 045802 (2005).